



Raman spectral features of a natural chromitite from NW Türkiye: Characterization of magnesiochromite spectra and implications

Mehmet Akbulut

Dokuz Eylül University, Faculty of Engineering, Department of Geological Engineering, Central Campus, 35390, Buca-İzmir, Türkiye

ARTICLE INFO

Submitted: January 2025

Accepted: March 2025

Available on line: March 2025

* Corresponding author:
makbulut@deu.edu.tr

Doi: 10.13133/2239-1002/18803

How to cite this article:
Akbulut M. (2025)
Period. Mineral. 94, 21-36

ABSTRACT

In this work, a first detailed Raman spectroscopic measurement study of natural magnesiochromites from a multi-textural ophiolitic chromitite sample from Harmancık district in north-western Türkiye has been presented to characterize the Raman spectral features of Turkish high-Cr ophiolitic chromitites. The magnesiochromites in the multi-textural chromitite sample has an almost uniform composition, with Cr_2O_3 , Al_2O_3 , and TiO_2 contents being 62.02 wt%, 9.18 wt%, and 0.14 wt% in average, respectively. Cr#s are 0.82 and Mg#s are 0.65 in average, in the ranges that of typical ophiolitic chromitites of boninitic to arc-related affinity. Despite this uniform composition, three distinctive Raman spectra morphologies (Types I, II and III) are determined. Of these, the Type I spectra is by far the dominant. Three common main band clusters are defined (BG-I, BG-II and BG-III) for all of the morphological types. The BG-I ($\sim 385\text{-}605\text{ cm}^{-1}$) and BG-II ($\sim 649\text{-}739\text{ cm}^{-1}$) are the main clusters that incorporate the high intensity and descriptive peaks and shoulders. The BG-III includes the very low intensity broad bands around $1122\text{ to }1763\text{ cm}^{-1}$, considered as overtones of the BG-I, and BG-II. Four of the several bands in the BG-I and BG-II has been assigned to the A_{1g} ($\sim 690\text{ cm}^{-1}$), $F_{2g}(3)$ ($\sim 605\text{ cm}^{-1}$), $F_{2g}(2)$ ($\sim 555\text{ cm}^{-1}$), and E_g ($\sim 470\text{ cm}^{-1}$) modes of spinel. Of the several un-assigned bands, the $\sim 730\text{ cm}^{-1}$ band has been interpreted to be related with the high-Cr nature of the studied sample. The variance in this band's intensity has been interpreted to be related with concomitant or post-crystallization textural arrangement and the plastic mantle deformation. This result emphasize the viability of a preliminary approach on orientation of the magnesiochromites in the ophiolitic chromitites via Raman spectroscopy, if the composition variable can be constrained.

Keywords: magnesiochromite; ophiolitic chromitites; Raman spectroscopy; band assignment; north-western Türkiye.

INTRODUCTION

Certain types of ore deposits need precise acquisition of the descriptive characteristics of ore minerals in order to construct a clear understanding of the ore-forming processes. This especially, is important for the only sources for the strategic chromium metal, the chromite deposits (a.k.a., chromitites) where the characterization of chrome

spinel (chromite, magnesiochromite and zincochromite of the spinel group) is an utmost tool for understanding the genesis and environment of occurrence. The chemical composition of the natural chrome spinel varies widely as the A and B cations in its AB_2O_4 structure corresponds to a large variety of divalent and trivalent ions (A: Fe^{2+} , Mg^{2+} , Mn^{2+} , Zn^{2+} and B: Cr^{3+} , Al^{3+} and Fe^{3+} , respectively).

This variance allows tracking of the magmatic and/or metasomatic processes that have been effective during its formation and following post-magmatic stages.

Most applied in-situ analytical methods for chemical characterization of chrome spinel are the electron probe micro-analysis (EPMA), and the laser-ablation inductively coupled plasma mass-spectrometry (LA-ICP-MS). However, Raman spectroscopy is also being explored as an additional useful method for characterization of the spinels for some time. Raman spectroscopy works by laser-excitation of the target of interest and detection of the scattering to reveal the Raman-active vibrational transitions, providing a suitable set of data for detection/characterization of mineral phases in geologic occurrences. The vibrational modes create bands (peaks) in the Raman spectra and observation of the characteristic band positions helps to identify the target phase. Additionally, variation in the spectral band positions and widths (full width at half maximums-FWHMs) reflect the target phase's compositional variation and/or stress/strain, and crystallinity state, respectively. Hence, for characterization of Raman features of the chrome spinel, a holistic handling of spectra is necessary. In this context, research on Raman spectroscopic data for natural and synthetic spinels, and several solid solutions characterizing the spinel group system has been ongoing for decades making up a large literature including determination of characteristics of spectra, Raman-active modes, and spectral modifications in relation to the compositional variance of the group members (e.g. McCarty and Boehme, 1989; Malézieux et al., 1983; Wang et al., 2002; Reddy and Frost, 2005; Yong et al., 2012; Lenaz and Skogby, 2013; Lenaz and Lughi, 2013, 2017; D'Ippolito, et al., 2015; Kharbish, 2018, Kaliwoda et al., 2021). This literature summarizes that Raman spectroscopy may be an important method for research on the formation of chromitites.

To the author's knowledge, there are no comprehensive Raman spectral datasets from chrome spinel of the Turkish ophiolitic chromitites. One Raman spectral dataset in the literature presents composite Raman spectra obtained during laser-excitation of minute lamellar diopside inclusions within magnesiochromite (cf. Akbulut, 2018). Nevertheless, in that work Akbulut (2018) has discussed the magnesiochromite band positions in the composite spectra only to describe the determinative band positions for the diopside micro-lamellae.

This current study aims to present a first detailed dataset of Raman spectral features from magnesiochromite grains of Turkish chromitites. For this purpose, a single natural high-Cr chromitite sample from north-western Türkiye is selected. The selected sample provided from a chromite mine in Harmancık (Bursa, NW Türkiye) includes dunitic orbicular (a.k.a. grapeshot ore, cf. Bilgrami, 1963), semi-

massive and massive textures, and was discussed earlier by Akbulut (2018). Both compositional and Raman spectral datasets of unzoned and fresh chrome spinel grains from several selected parts are gathered from this single sample, in an attempt to omit the spinel chemistry variable that is a strong control on Raman band positions. By this, it is aimed to leave more room for discussions on other constraining features for the Raman spectra, as unaltered magnesiochromite grains in a given single chromitite sample is usually expected to present almost homogenous chemical compositions. This work hopes to be a start-up for future possible work for describing characteristic features of Raman spectra for Turkish ophiolitic chromitites, and expects to contribute to the growing literature on Raman spectroscopy of geological materials.

GEOLOGICAL SETTING AND DESCRIPTION OF THE SAMPLE MATERIAL

The geological setting of modern Türkiye is an outcome of the closure of the Tethys Ocean and the formation of the mid-western segment of the Alpine-Himalayan Orogeny during Palaeozoic and Cenozoic (Figure 1a). This complex closure process has resulted in occurrence of three main suture zones (Izmir-Ankara-Erzincan, Inner-Tauride, and Bitlis-Zagros Suture Zones; Figure 1b). These suture zones mark the amalgamation fronts of the continental and oceanic fragments of the Tethys realm and can be traced along E-W trending three main ophiolitic belts, namely the northern, Tauride and peri-Arabic ophiolitic belts (Figure 1b). These ophiolite belts are generally composed of tectonically emplaced fragments of the oceanic crust and lithospheric mantle (ophiolites) and their intensely tectonized counterparts (ophiolitic mélanges). The peridotite massifs of these belts, comprising the ultramafic cumulates and the mantle tectonites, host a significant number of ophiolitic chromitite occurrences that are long-time exploited as high-quality chromium metal sources.

One of these peridotite massifs is found at the north-western part of the northern ophiolite belt, around Harmancık (Bursa, NW Türkiye; Figure 1 b,c). These peridotite nappes of mantle tectonites, mainly made of moderately to strongly serpentinized harzburgite and dunites that have thrust over the Palaeozoic HP-LT metamorphic basement rocks (blueschists and accompanying recrystallized carbonates) of the Tavşanlı zone during Upper Cretaceous era with the subduction of the Neotethyan oceanic realm (cf. Uysal et al., 2014 and the references therein, and Akbulut, 2018). The ophiolitic chromitites of the Harmancık peridotites occur within the dunitic hosts accompanied and surrounded by harzburgites, and form pods, lenticular and tabular shaped geometries, and occasional schlieren structures

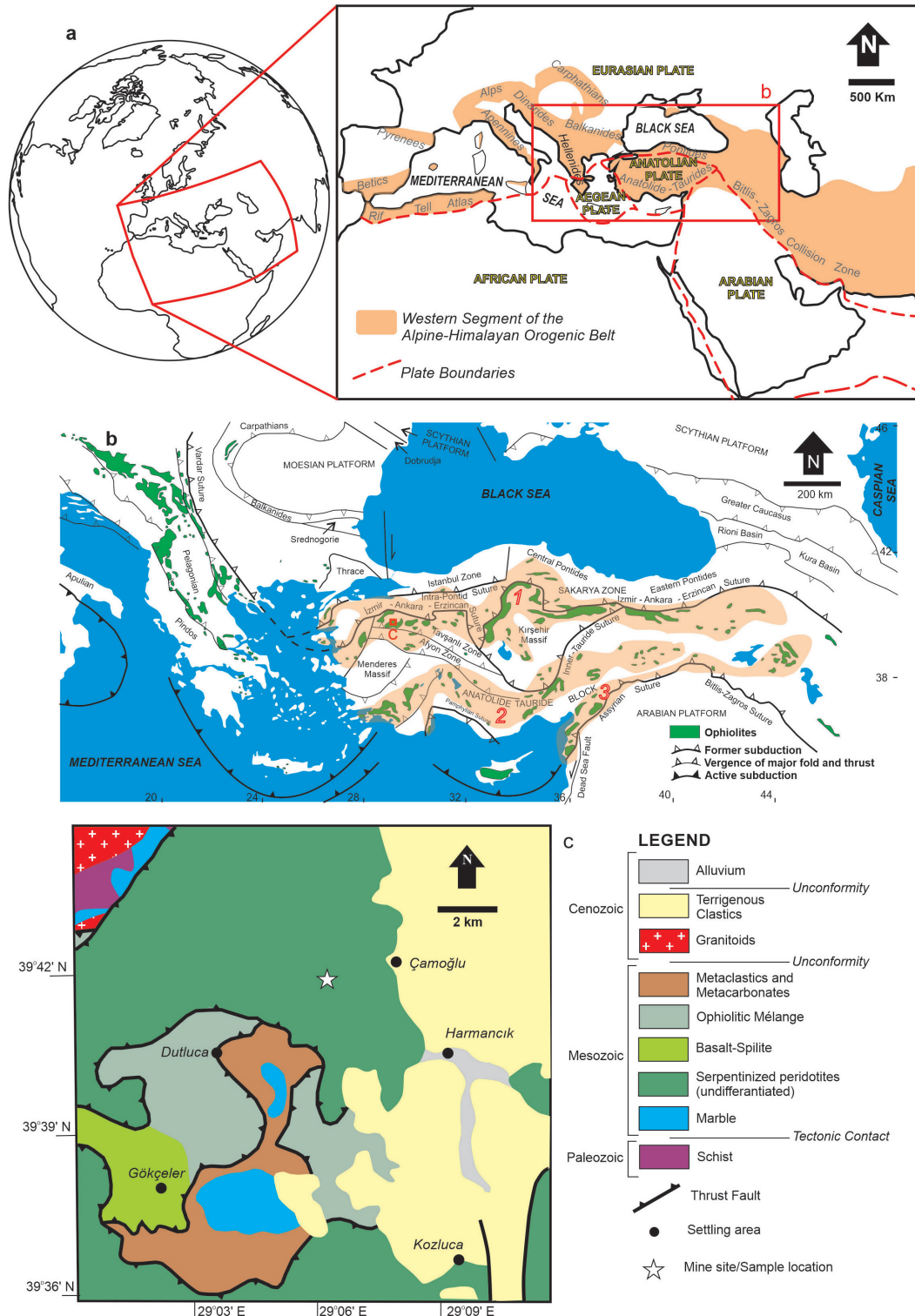


Figure 1. a) Globe and map sketches illustrating the location and distribution of the western segment of the Alpine-Himalayan Orogenic Belt. b) Paleotectonic terranes and major sutures of the Eastern Mediterranean (after Tavlan et al., 2011 and Akbulut, 2018). The northern, Tauride, and the peri-Arabic ophiolitic belts (1, 2, and 3, respectively) of Türkiye are roughly traced along the ophiolites. c) Simplified geological map of the surroundings of the source mine site, after Akbulut (2018) who established the imagery from Geoscience Map Viewer and Drawing Editor of General Directorate of Mineral Research and Exploration (MTA) that utilize the compilation of geological map of Türkiye by Akbaş et al. (2001).

that present disseminated, semi-massive, massive, nodular, and rare orbicular chromite textures typical to the ophiolitic chromitites (cf. Akbulut, 2018). Any or all of these textures can be found in a given chromitite specimen. During Neogene, these peridotite nappes has been unconformably covered by terrestrial sediments and accompanying coal formations (Uysal et al., 2014), and later, all these lithostratigraphic units are unconformably overlain by Quaternary deposits.

The chromitite sample studied in this work was provided by the company officials of a chromite mine located just northwest of Harmancık town (Bursa, north-western Türkiye, Figure 1c). The sample including dunitic orbicular, semi-massive and massive ore segments was described earlier by Akbulut (2018) in detail. The orbicules are composed of spherical/elliptical dunitic shells surrounding almost silicate-free chromite

nodule cores (Figure 2 a,b). These dunitic orbicules with chromite nodule cores are surrounded by a concomitant and/or following stage of chromite accumulation that is densely packed outwards gradually. This forms a semi-massive to massive chromitite envelope for the dunitic orbicules. Akbulut (2018) notes that the accumulation semi-massive to massive chromitite envelope also seems to have resulted in flattening of the dunitic shells finally resulting in their structural failure and incorporation in the massive chromitite. Akbulut (2018) had inquired the textural and other observations on the sample for possible macroscopic clues on deep-mantle recycling processes; however, he could not reach to a definitive conclusion due to conflicting findings. Hence, the textural observations in this study will only be considered descriptive for a multi-stage formation process that incorporates at least one semi-plastic deformation stage.



Figure 2. a) and b) Images of the studied chromitite sample with intriguing dunitic orbicular texture.

ANALYTICAL METHODS

Selected pieces of ore segments from the studied sample were cut, were embedded in epoxy resin, and then polished. Four ore blocks (sample blocks 1 to 4), polished at the Dokuz Eylül University Geological Engineering Department (Izmir, Türkiye), were subjected to petrographic, compositional and spectroscopic analysis. Reflected light microscopy work for the areas of interest was conducted at the same facility using Leica DM2500P and Nikon E400POL microscopes. A special care was taken for the selection of these areas, in order to take the chromite grains from different textural segments into account.

Chromite grains in those areas of interest (e.g., Figure 3 a,k) were analysed for their major elemental compositions by a JEOL JXA-8230 electron micro-probe (EPMA) in Central Laboratory of Middle East Technical University (Ankara, Türkiye). EPMA analysis were completed from 36 points. 20 kV acceleration voltage and 5 μ probe diameter were selected. Standards for Mg, Al, Fe, and Ti elements were selected as MgO, Al₂O₃, Fe₂O₃ and TiO₂, respectively. Wollastonite and rhodonite were set as Si and Mn standards. Metals of Ni, Zn, Cr, and V were used for Ni, Zn, Cr, and V elements, respectively.

Micro-Raman spectroscopy of the chromites were made in Central Research Laboratory of Izmir Katip

Çelebi University (Türkiye) utilizing a Renishaw inVia Confocal Raman Microscope and Spectrometer. 35 of the spots targeted during the EPMA work were analysed. The excitation source utilized was a 532 nm laser. Grating was set as 2400 line/mm, and 20x to 100x objectives were used. Laser power impinging on the sample surface is set to 2.5 mW. Cosmic-Ray Events (CRE) peaks were removed using CrystalSleuth software (Laetsch and Downs, 2006). Related literature and RRUFF Raman spectra database (<http://rruff.info>) were checked for inquiry and selection of determinative bands for magnesiochromites. Band deconvolution of the selected 17 obtained spectra were made by Fityk software v. 1.3.1 (Wojdyr, 2010), utilizing Voigt function after baseline treatment. Degrees of freedom applied were between 2813 and 2843. The curve-fitting process was iteratively performed using Levenberg-Marquardt (LM) method until no better fit could be obtained. The fitting performance for each spectrum was evaluated via the reduced- χ^2 and R² values calculated for each fit.

RESULTS

Representative mineral chemistry and Raman spectroscopy data of the studied magnesiochromites in this work are briefly introduced in the Tables 1 and 2, and Figures 4 and 5, respectively. Additional

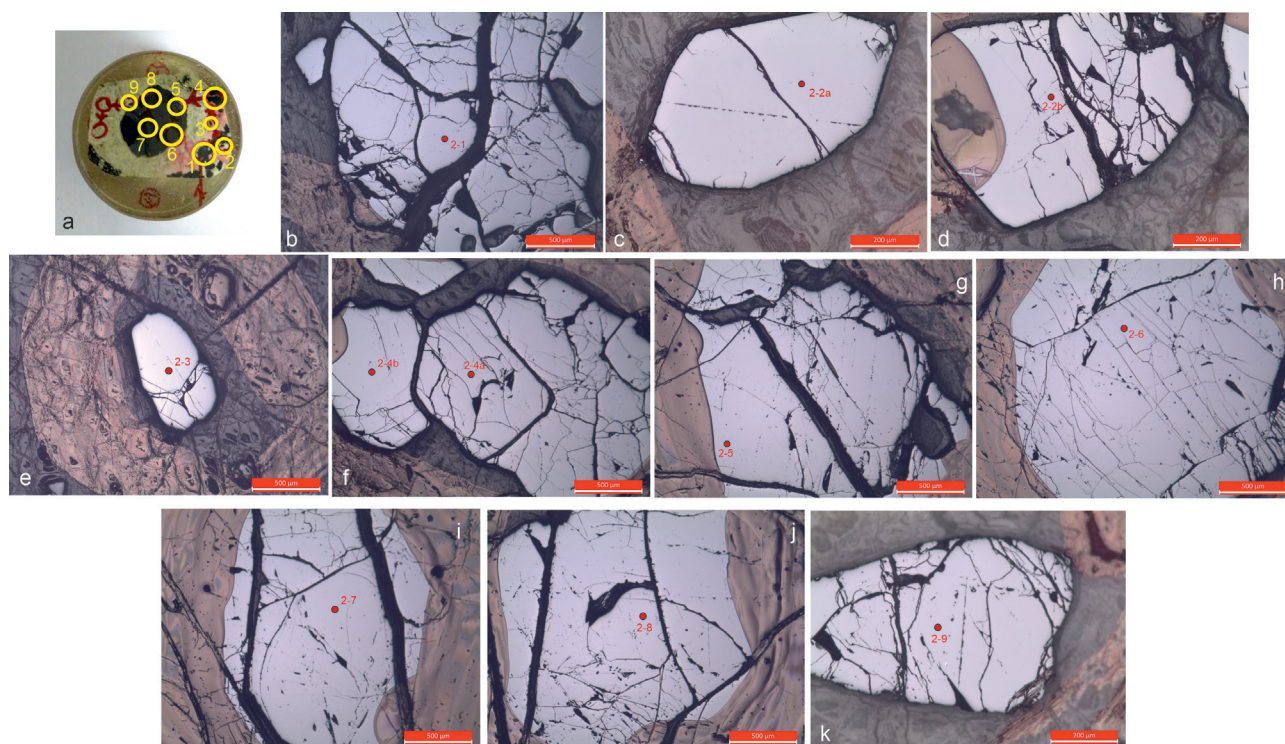


Figure 3. a) Exemplary analytical areas of interest marked with yellow circles on the polished chromitite block. b) to k) shows examples of the analytical points on chrome spinels which are used both for electron probe micro-analysis (EPMA) and Raman spectroscopy.

Table 1. Selected wavelength dispersive spectrometry (WDS) data from the electron probe micro-analysis (EPMA) of analysed magnesiochromites and additional magnesiochromite data from the RRUFF library (<https://rruff.info/magnesiochromite>) given for comparison.

Sample	2-1	2-2A	2-2B	2-3	2-4A	2-4B	2-5	2-6	2-7	2-8	2-9	R050399	R060796	R060797
	sur	sur	sur	sur	sur	sur	nod	nod	nod	nod	sur			
SiO ₂	0.01	0.00	0.00	0.02	0.00	0.02	0.01	0.00	0.00	0.00	0.00	-	-	-
TiO ₂	0.14	0.13	0.16	0.12	0.13	0.13	0.14	0.13	0.16	0.12	0.12	-	0.09	0.43
V ₂ O ₅	0.12	0.09	0.07	0.09	0.07	0.10	0.09	0.09	0.11	0.07	0.07	-	-	-
Al ₂ O ₃	9.10	9.08	9.09	9.25	9.06	9.17	9.29	9.25	9.32	9.16	9.17	17.03	10.29	14.62
Cr ₂ O ₃	62.17	62.33	61.83	61.72	61.82	62.10	62.25	62.18	62.02	62.69	61.24	50.83	56.26	47.71
FeO _l	15.30	15.21	15.36	15.32	14.83	15.05	15.01	14.64	15.14	14.72	17.14	14.94	18.16	21.97
MnO	0.07	0.09	0.09	0.11	0.38	0.36	0.07	0.07	0.06	0.07	0.34	-	-	-
MgO	13.41	13.55	13.28	13.56	13.48	13.66	13.56	13.79	13.61	13.30	12.19	14.74	11.51	11.85
NiO	0.15	0.14	0.12	0.12	0.11	0.14	0.12	0.09	0.16	0.10	0.11	-	-	-
ZnO	0.11	0.04	0.04	0.01	0.05	0.03	0.05	0.07	0.02	0.01	0.10	-	-	-
Total	100.58	100.66	100.05	100.31	99.93	100.76	100.59	100.32	100.59	100.24	100.49	97.54	96.31	96.58
Cr# (Cr/Cr+Al)	0.82	0.82	0.82	0.82	0.82	0.82	0.82	0.82	0.82	0.82	0.82	0.67	0.79	0.69
Mg# (Mg/Mg+ Fe ²⁺)	0.65	0.65	0.64	0.65	0.66	0.66	0.65	0.66	0.65	0.64	0.60	0.70	0.58	0.57
Fe ²⁺ # (Fe ²⁺ /Fe ²⁺ +Mg)	0.35	0.35	0.36	0.35	0.34	0.34	0.35	0.34	0.35	0.36	0.40	0.30	0.42	0.43
Fe ³⁺ # (Fe ³⁺ /Fe ³⁺ +Cr+Al)	0.03	0.03	0.03	0.03	0.03	0.03	0.03	0.03	0.03	0.02	0.03	0.05	0.04	0.09
(Cr+Fe ³⁺)/(Cr+Fe ³⁺ +Al)	0.83	0.83	0.83	0.82	0.83	0.83	0.82	0.82	0.82	0.82	0.82	0.68	0.80	0.71

(sur): magnesiochromite in the surrounding chromite accumulation; (nod): magnesiochromite in the nodular core of the dunitic orbicule. Samples denoted with italic fonts are magnesiochromites from the RRUFF library (<https://rruff.info/magnesiochromite/R050399>; <https://rruff.info/magnesiochromite/R060796>; and <https://rruff.info/magnesiochromite/R060797>) and are provided here for comparison and discussions. See text for details.

Table 2. List of Raman bands obtained via deconvolution of selected Raman spectra of studied magnesiochromites. Bands deconvoluted from the raw Raman spectra of unoriented (*) and oriented (**) magnesiochromite samples from the RRUFF library (<https://rruff.info/magnesiochromite>) is presented for comparison.

Spectrum Morphology	Analytical Spot	Grain type	Tests for goodness of fit																
			Band Group I			Band Group II			Band Group III			reduced- χ^2	R ²	Cr#	Mg#	(Cr+Fe ³⁺)/(Cr+Fe ³⁺ +Al)			
Assigned vibrational modes			E _g	F _{2g} (2)	F _{2g} (3)	A _{1g}													
Type I	2-1	sur	400	477	557	579	602	650	<u>691</u>	724	1127	-	-	-	1.0416	0.9967	0.82	0.65	0.83
	2-2b	sur	391	474	557	582	604	649	<u>691</u>	724	1127	-	1397	-	0.9138	0.9968	0.82	0.64	0.83
	2-3	sur	391	477	554	579	603	650	<u>691</u>	717	1131	-	-	-	0.9127	0.9965	0.82	0.65	0.82
	2-4a	sur	395	476	556	579	602	649	<u>691</u>	706	1134	-	-	-	0.9255	0.9971	0.82	0.66	0.83
	2-9	sur	395	474	557	580	602	649	<u>691</u>	724	1122	-	-	-	1.0449	0.9972	0.82	0.60	0.82
	2-4b	sur	398	473	555	578	602	650	<u>691</u>	725	1130	-	1390	-	1.0217	0.9968	0.82	0.66	0.83
	2-5	nod	392	476	553	580	605	650	<u>691</u>	723	1126	1285	1388	-	1.0024	0.9973	0.82	0.65	0.82
	<i>R060797*</i>		-	468	548	576	600	648	<u>686</u>	704	1090	-	-	-	0.5569	0.9921	0.69	0.57	0.71
	<i>R060796*</i>		-	-	558	576	597	651	<u>694</u>	737	1104	-	-	-	0.6408	0.9890	0.79	0.58	0.80
Type II	2-2a	sur	401	468	553	580	605	650	<u>692</u>	734	1128	-	-	-	0.9499	0.9961	0.82	0.65	0.83
	2-6	nod	393	478	555	580	604	651	<u>692</u>	730	1127	-	-	-	1.0791	0.9976	0.82	0.66	0.82
	2-7	nod	385	475	555	581	604	650	<u>692</u>	736	1127	-	1422	1763	0.8764	0.9362	0.82	0.65	0.82
Type III	2-8	nod	-	457	552	578	605	654	697	<u>739</u>	1139	-	-	1449	1.1256	0.9972	0.82	0.64	0.82
	<i>R050399*</i>		-	453	558	586	608	654	<u>698</u>	742	-	-	-	-	0.0177	0.9993	0.67	0.70	0.68
	<i>R050399**</i>		-	519	563	581	610	658	<u>701</u>	740	1139	1178	-	-	1.1574	0.9987	*	*	*

(sur): magnesiochromite in the surrounding chromite accumulation; (nod): magnesiochromite in the nodular core of the dunitic orbicule. (*): Raman data from the unoriented magnesiochromites, obtained from the RRUFF library (<https://rruff.info/magnesiochromite/R060796>; <https://rruff.info/magnesiochromite/R060797>). (**): Raman data (depolarized) from the oriented magnesiochromite from the RRUFF library, where laser is oriented parallel to a* (1 0 0), fiducial mark perpendicular to laser parallel to c [0 0 1] (<https://rruff.info/magnesiochromite/R050399>). RRUFF spectra are deconvoluted according to the same methodology used for the analytical runs in this study. Underlined bands mark the strongest (highest intensity) bands for each spectrum. All Raman band values are in cm⁻¹.

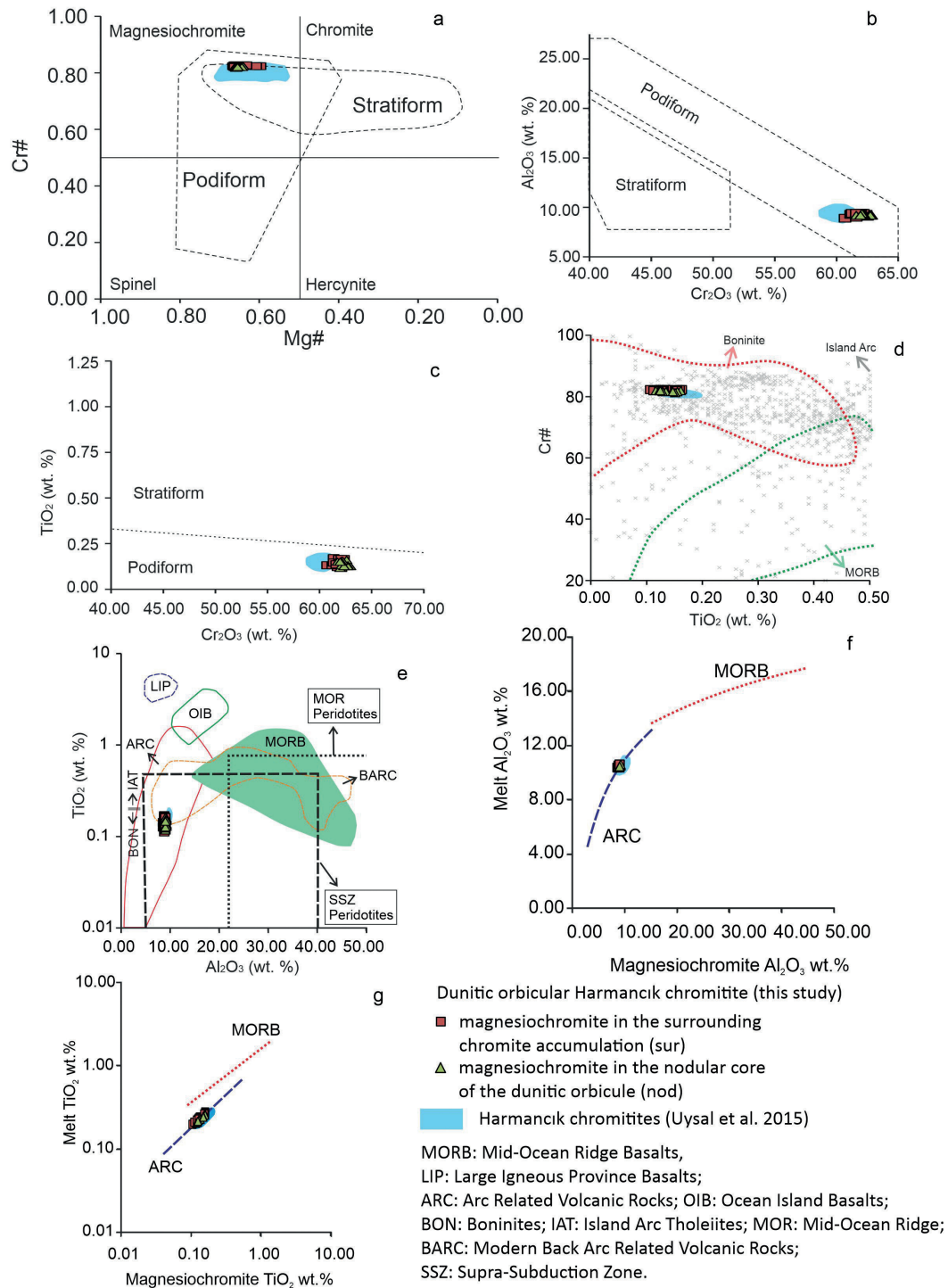


Figure 4. Distribution of the major oxide data of the studied chromite grains and estimated parental melt composition on the bivariate plots of a) Cr# [Cr/(Cr+Al)] vs Mg# [Mg/(Mg+Fe²⁺)], b) Al₂O₃ (wt%) vs Cr₂O₃ (wt%), c) TiO₂ (wt%) vs Cr₂O₃ (wt%), d) Cr# vs TiO₂ (wt%), e) TiO₂ (wt%) vs Al₂O₃ (wt%), f) (Al₂O₃)_{melt} vs (Al₂O₃)_{magnesiochromite}, and (g) (TiO₂)_{melt} vs (TiO₂)_{magnesiochromite}. (nod): magnesiochromite in the nodular core of the dunitic orbicule, (sur): magnesiochromite in the surrounding chromite accumulation. Fields marked in (d) and (e) are from Barnes and Roeder (2001) and Kamenetsky et al. (2001), respectively. Regression trends in (f) and (g) are from Rollinson (2008). Sky blue fields on all of the plots show distribution of data for Harmancik chromitites presented earlier by Uysal et al. (2015).

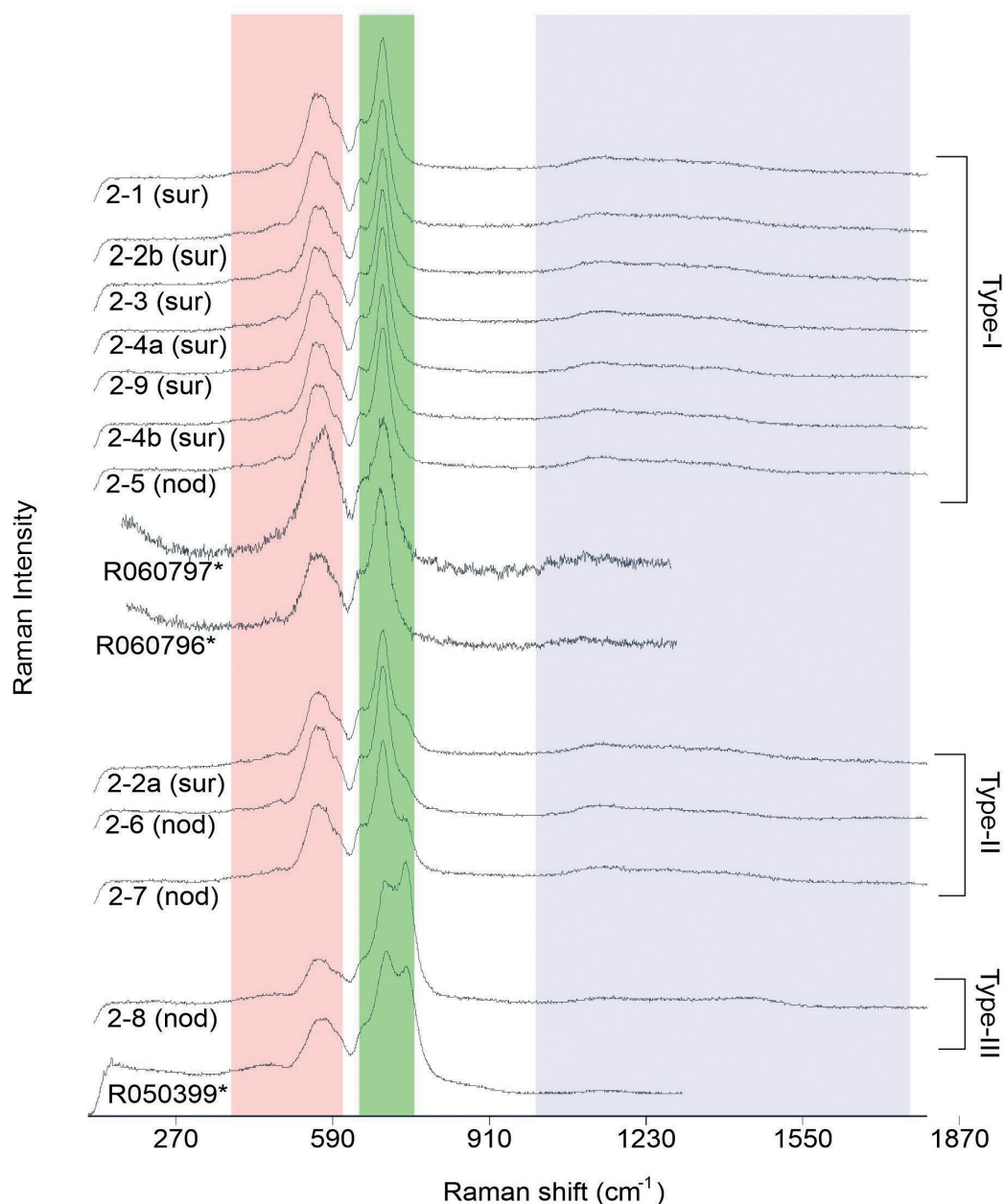


Figure 5. Examples of three morphological types of raw (non-baseline treated) Raman spectra obtained from the analytical runs. Raw Raman spectra marked with asterisk symbol (*) are unoriented magnesiochromites from the RRUFF library (<https://rruff.info/magnesiochromite>), and are given for comparison with the corresponding morphological type interpretations. See the text for the description on their texture, and Tables 1 and 2 for their compositional and Raman data. The pink, green, and light purple regions in the figure corresponds to the described Band Groups I, II, and III, respectively. Abbreviations next to the sample names analysed in this study are as in Figure 4.

magnesiochromite mineral chemistry and raw Raman spectral data from unoriented and oriented magnesiochromite samples are obtained from the RRUFF library (<https://rruff.info/magnesiochromite>) and included in these tables and figures for comparison (R050399, R060796, and R060797). R050399 data is from a coarse

granular chromite grain surrounded by a silicate matrix in a semi-massive chromitite. R060796 data is from a chromite in a fine-grained massive chromitite, and R060797 data is from a chromite in a coarse-grained (granular) massive chromitite.

Mineral Chemistry

Uysal et al. (2015) reports that the Harmancik chromitites are made of magnesiochromites that present Cr_2O_3 , Al_2O_3 , and TiO_2 values between 59.24-61.27 wt%, 9.09-10.03 wt%, and 0.14-0.18 wt%, respectively. Their Cr/(Cr+Al) atomic ratios (Cr#s) are also calculated to be 0.80-0.82, and the Mg/(Mg+Fe²⁺) atomic ratios (Mg#s) to be between 0.59-0.69 (Uysal et al., 2015).

The analysis of magnesiochromites in the current study also show very similar compositions with these previously reported compositional ranges. Overall, the major oxide data obtained from all 36 points on the four polished blocks clearly mark an almost uniform chemical composition, free of chemical variance as well as zoning, in all the textural types of the magnesiochromites analysed in the sample. They present Cr_2O_3 , Al_2O_3 , and TiO_2 values between 60.77-62.83 wt%, 8.84-9.41 wt%, and 0.11-0.17 wt%, respectively, and their Cr#s and Mg#s are high, between 0.79-0.83 and 0.53-0.67 (Table 1). All of the magnesiochromites fall in the analytical ranges pronounced for typical ophiolitic (podiform) chromitites (Figure 4 a,c). The Cr#s of the magnesiochromites from the nodules at the cores of the dunitic orbicules and the enveloping chromitite is almost constant. All of the magnesiochromites show a Ti-poor and high Cr-character and reflect a boninitic to arc-related affinity (Figure 4 d,e). The Al_2O_3 and TiO_2 contents of the parental magma, empirically estimated utilizing the equations $(\text{Al}_2\text{O}_3)_{\text{melt}} = 5.2181 \ln(\text{Al}_2\text{O}_3)_{\text{sp}} - 1.0505$ and $(\text{TiO}_2)_{\text{melt}} = 1.0963(\text{TiO}_2)_{\text{sp}}^{0.7863}$ (e.g., Rollinson, 2008; Rollinson and Adetunji, 2015), range between 10.32-10.65 wt% and 0.19-0.27 wt%, respectively. These ranges plot on and follow clearly the regression lines of the arc-related chromites (Figure 4 f,g).

Raman Spectroscopy

Figure 5 shows the representative raw (non-baseline treated) Raman spectra from the magnesiochromites studied. One of the distinctive features of these raw spectra is the clear presence of different morphologies despite the lack of significant chemical variations. Three distinctive Raman spectra morphologies are determined in this study. They are named as Type I, Type II, and Type III largely on the basis of the band intensity variations. The dominant morphology encountered in all of the 35 analytical runs from all of the polished blocks was Type I spectra (n=30). Only four (4) Type II and one (1) Type III spectra are determined. All three of the spectra types are detected only in the sample block 2 (Figure 3). As this block includes all types of chromitite textures within the sample, Figure 5 comprises data from this sample block, in order to summarize and compare the spectral diversity with respect to the textural positions of the magnesiochromites. Type I, and Type II spectra are determined from analytical runs

on magnesiochromite grains in both the semi-massive to massive chromitite accumulation envelope and the nodular cores of the dunitic orbicules. The single Type III spectrum determined is found only in the nodular core of the dunitic orbicule in sample block 2 (Figures 3 and 5).

Regardless of its morphological type, all of the Raman spectra presented in this study show high intensity bands ranging in the characteristic spectral region defined for the oxide species (ca. 300-700 cm^{-1} , cf. Wang et al., 1994). Two significant band clusters are identified around the wavenumbers 385-605 cm^{-1} (Band Group I, BG-I) and 649-739 cm^{-1} (Band Group II, BG-II) (Table 2, Figure 6 a,d). The strong (high intensity) bands are generally incorporated within these two clusters. Another third band set (Band Group III, BG-III) including very low intensity broad bands are detectable around 1122 to 1763 cm^{-1} .

In all morphological types of spectra, the BG-I is represented by three main bands, a medium intensity broad peak at $\sim 555 \text{ cm}^{-1}$, a distinct lower intensity shoulder band at $\sim 605 \text{ cm}^{-1}$, and a connecting band in-between at $\sim 580 \text{ cm}^{-1}$. Two additional very low intensity broad bands at $\sim 470 \text{ cm}^{-1}$ and $\sim 395 \text{ cm}^{-1}$ accompanies these three main bands. The BG-II similarly includes three main bands, at $\sim 650 \text{ cm}^{-1}$, $\sim 690 \text{ cm}^{-1}$, and 730 cm^{-1} . The $\sim 650 \text{ cm}^{-1}$ band always forms a medium intensity distinct shoulder, and the band at $\sim 690 \text{ cm}^{-1}$ always forms a high intensity narrow peak. However, the intensity of the shoulder band at $\sim 730 \text{ cm}^{-1}$ is variable. Intensity of this band increases from Type I to Type II spectra (Figure 6 a,b), and exceeds that of the $\sim 690 \text{ cm}^{-1}$ band in the Type III spectra (Figure 6d). Setting aside this final diversion in the band intensities, the band positions in all spectra are almost invariable, most probably due to the lack of compositional variety in the grains analysed.

DISCUSSION: BAND ASSIGNMENTS AND IMPLICATIONS

For a proper understanding of the Raman spectral features of a mineral, it is important to check the characteristic spectral region in order to determine the strongest band, which is described to usually correlate with the totally symmetric vibrational mode (TS mode) of the strongest covalent bond of investigated phase (Wang et al., 1994). The Raman-active vibrational modes for spinel (AB_2O_4) are generally defined to be $\text{A}_{1g} + \text{E}_g + 3\text{F}_{2g}$ (e.g., White and De Angelis, 1967; Malézieux et al., 1983; Wang et al., 1994; Kharbish, 2018; D'Ippolito et al., 2015; Naveen et al., 2019). However, it should also be noted that up to three additional bands are repeatedly reported in both synthetic MgAl_2O_4 (e.g., Fraas et al., 1973; Malézieux et al., 1983) and natural magnesiochromites (e.g., Malézieux et al., 1983; Kharbish, 2018).

The strongest covalent bonds in spinel are the $\text{B}^{3+}\text{-O}$ bonds of the ${}^{\text{M}}\text{BO}_6$ octahedron (where B refers to Cr^{3+} , Al

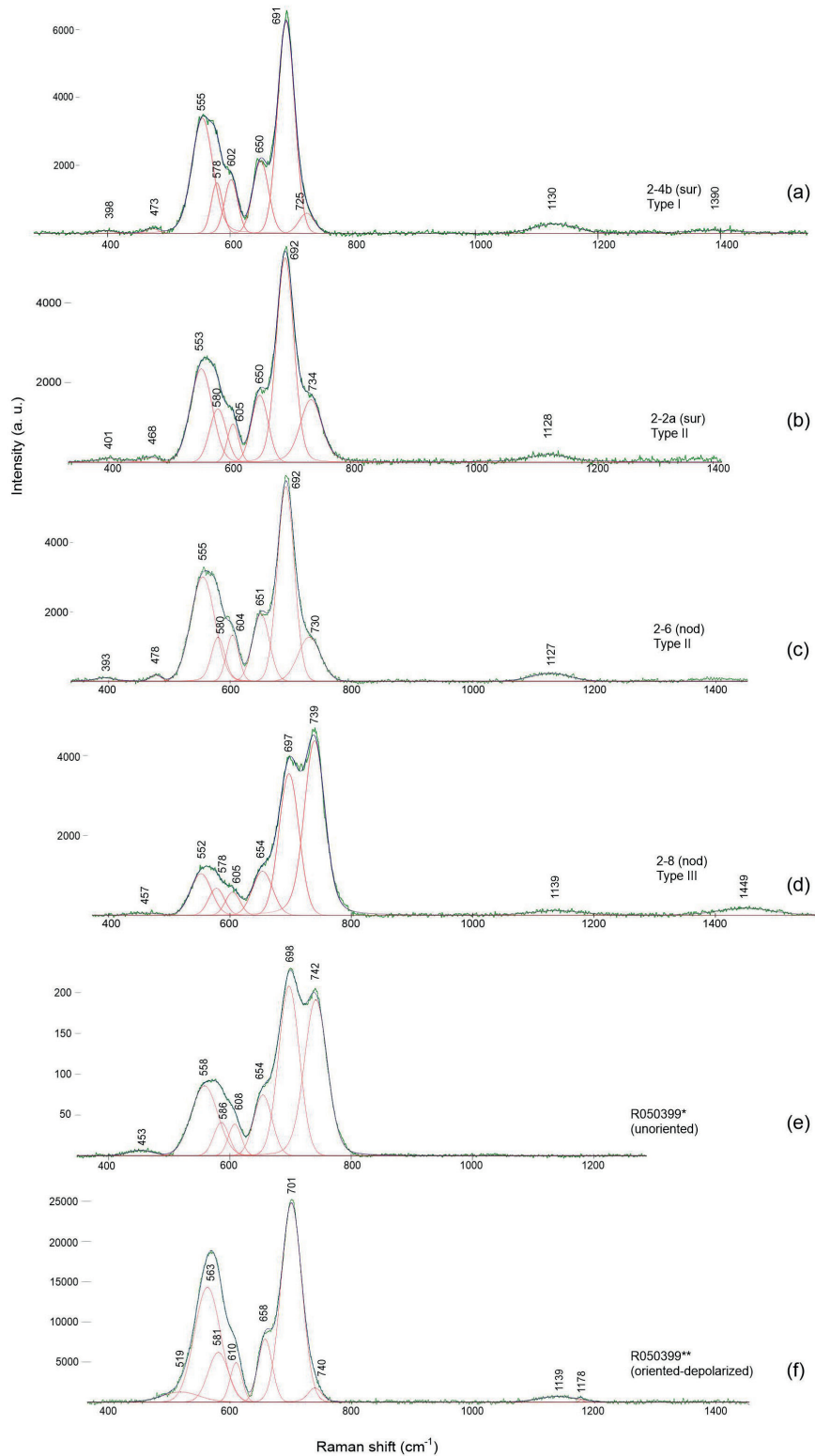


Figure 6. a-d) Representative deconvoluted spectra from this study, and e-f) deconvolution results of magnesiochromites from the RRUFF library (<https://rruff.info/magnesiochromite>) given for comparison. Green lines denote data from analytical runs. Red curves are the functions used for fitting the data and the blue lines stacking with the green analytical data line is the final best-fit model. See Figure 4 and Tables 1 and 2 for the sample abbreviations.

and Fe^{3+}), and vibration of these bonds mainly contribute to the TS mode (cf. Kharbush, 2018 and the references therein), which also corresponds to the A_{1g} mode in spinel (cf. Wang et al., 1994). Remaining less intense modes reported in the literature are usually reported to be in the sequence of $F_{2g}(3) > F_{2g}(2) > E_g > F_{2g}(1)$ (e.g., D'Ippolito et al., 2015; Kharbush, 2018 and the references therein; Naveen et al., 2019). Additionally, it has been suggested that the E_g peak positions are helpful in deciphering the subgroups of the analysed spinels, as the E_g modes at ~ 450 , ~ 400 , and < 380 cm^{-1} wavenumbers are debated to be characteristic for the chromate, aluminate, and ferrite spinels, respectively (cf. D'Ippolito et al., 2015; Lenaz and Lughi, 2017). Accordingly, the assignment of the bands obtained via deconvolution of the magnesiochromite spectra in this work is done following these mentioned criteria (Table 2).

A_{1g} Mode

The wavenumber of the strongest (highest intensity) mode in Type I and Type II spectra, the narrow and well-defined band at ~ 690 cm^{-1} (with only a 0.14% Raman shift variation), is in good agreement with the strongest bands described from earlier work (e.g., Wang et al., 2002; Yong et al., 2012; D'Ippolito, et al., 2015; Kharbush, 2018; Naveen et al., 2019; Nayak et al., 2024). Hence, for Type I and Type II spectra, this band may easily be correlated with the A_{1g} (a.k.a. TS) vibrational mode resulting from symmetric stretching of the spinel ${}^M\text{BO}_6$ octahedra (cf. Kharbush, 2018). However, in the Type III spectrum, the strongest band is at 739 cm^{-1} (Figures 5 and 6, Table 2) despite the ~ 690 cm^{-1} band also being clearly visible as the second highest intensity band with only a slight ($\sim 1\%$) Raman shift variance (at 698 cm^{-1}). This band shift variation is still within a very narrow range, and there are no significant band shift changes in the other bands. Up to 9% Raman shifts are reported in the position of the modes in the chromate spinels (e.g., D'Ippolito et al., 2015). Moreover, especially $\sim 7\%$ Raman shifts are reported in the position of the strongest bands of chrome spinels of variable chemical compositions (e.g., Kaliwoda et al., 2021). Thus, it is still probable to assign the ~ 690 cm^{-1} band of Type III spectrum to the A_{1g} mode. Making such an assignment for the strong ~ 690 cm^{-1} band however, requires an explanation for the co-existing highest intensity band at 739 cm^{-1} .

It is well known that, substitution of cations in the spinel result in significant changes in Raman spectra (Wang et al., 2004). For example, in their study on natural and synthetic chromites, Malézieux et al. (1983) have reported surfacing of a shoulder near 735 cm^{-1} for the natural chromites with Cr_2O_3 contents > 63 wt% (Wang et al., 2004). In strong resemblance, the Cr_2O_3 contents of all of the magnesiochromite grains in this

current study are also higher than 60 wt%, and all of their Raman spectra include ubiquitous shoulders (albeit with variable intensities) at ~ 730 cm^{-1} wavenumbers. This fact, congruent with the report of the Malézieux et al. (1983), suggests that the ~ 730 cm^{-1} bands of the studied magnesiochromites may be related with the high Cr_2O_3 contents of the magnesiochromite grains. Furthermore, intensities of these shoulders and their Raman shift values, seems to have low to moderate positive correlation with the Cr_2O_3 contents ($r=0.6516$, and $r=0.5585$ respectively; Table 3). Additional similar low to moderate positive correlation coefficients between the MgO contents and the full width at half maximums (FWHMs) of the ~ 730 cm^{-1} shoulders ($r=0.6614$) are also notable. On the other hand, FWHMs of the ~ 730 cm^{-1} shoulders also seem to show a moderate negative correlation with the total FeO contents ($r=-0.7515$), and a low to moderate negative correlation with the ZnO contents ($r=-0.5074$). The MnO contents also show a low to moderate negative correlation with the Raman shift values of this band ($r=-0.5782$). Such relations, although not being very definitive with the current dataset, re-emphasize the effect of the mineral composition on the final magnesiochromite spectra morphology, in conformation with the literature.

The effects of chemical variation of the spinels are also usually discussed on basis of the strong negative correlation of the A_{1g} peak position shifts and the $(\text{Cr}+\text{Fe}^{3+})/(\text{Cr}+\text{Fe}^{3+}+\text{Al})$ molar ratios (e.g., Malézieux et al., 1983; Wang et al., 2004; Naveen et al., 2019; Figure 7). The increasing $(\text{Cr}+\text{Fe}^{3+})/(\text{Cr}+\text{Fe}^{3+}+\text{Al})$ molar ratio of the spinel results in shifting of the Raman A_{1g} peak position towards lower wavenumbers. Although the calculated $(\text{Cr}+\text{Fe}^{3+})/(\text{Cr}+\text{Fe}^{3+}+\text{Al})$ molar ratios of the studied magnesiochromites are almost constant (anchored around 0.82), and there is only a slight shift in the A_{1g} peak positions, the data points fall on the field of data cluster established from the above mentioned earlier work. This significantly comply with both the earlier and this study's inferences on the importance and usefulness of the A_{1g} peak positions on estimations of the mineral composition. The high intensity A_{1g} peak is attributed to the presence of higher amount of Cr (heavier atomic mass, 51.996 u) over Al (lighter atomic mass, 26.982 u) (Naveen et al., 2019).

However, despite all these effects related to the high Cr contents and the site occupancies of the trivalent cations, it should be noted that Type III-like double summited spectra also exists for less Cr bearing magnesiochromites, such as the analytical runs for unoriented R050399 magnesiochromite sample from the RRUFF library (Tables 1 and 2, and Figures 5 and 6e). Deconvolution result of (depolarized) Raman spectrum from the oriented R050399 sample is also given in Table 2 and Figure 6f, which presents a comparable spectrum morphology

Table 3. Correlation coefficients (r) between the Raman shifts, peak intensities, and the FWHMs (Full Width at Half Maximums) for the shoulder bands at $\sim 730\text{ cm}^{-1}$ wavenumber in the magnesiochromite spectra and the relevant major oxide contents.

	SiO ₂	TiO ₂	V ₂ O ₅	Al ₂ O ₃	Cr ₂ O ₃	FeO _t	MnO	MgO	NiO	ZnO	Peak Intensity*	Raman Shift*	FWHM*
SiO ₂	1												
TiO ₂	-0.1920	1											
V ₂ O ₅	0.3730	0.3228	1										
Al ₂ O ₃	0.2553	0.0725	0.2798	1									
Cr ₂ O ₃	0.0403	0.0171	0.2195	0.0226	1								
FeO _t	-0.1059	-0.1139	-0.1553	-0.0752	-0.7714	1							
MnO	0.1088	-0.3068	-0.3545	-0.3491	-0.5433	0.3730	1						
MgO	0.2983	0.1726	0.4171	0.2140	0.6211	-0.9114	-0.3911	1					
NiO	0.3050	0.4724	0.7651	-0.0010	-0.0149	0.0437	-0.1276	0.2105	1				
ZnO	-0.1097	0.0886	0.1787	-0.2396	-0.3610	0.5394	0.1746	-0.5300	-0.0139	1			
Peak Intensity*	-0.4004	-0.2041	-0.2187	0.0831	<u>0.6516</u>	-0.3689	-0.3514	0.0933	-0.3006	-0.4623	1		
Raman Shift*	-0.2769	0.1894	0.2712	0.2913	<u>0.5585</u>	-0.0994	<u>-0.5782</u>	0.0612	0.0815	-0.1671	0.6440	1	
FWHM*	-0.1769	-0.1633	-0.1337	-0.0777	0.3626	<u>-0.7515</u>	-0.0673	<u>0.6614</u>	-0.1677	<u>-0.5074</u>	0.2615	-0.2788	1.0000

*: spectral features of the shoulder bands at $\sim 730\text{ cm}^{-1}$, FWHM: Full Width at Half Maximum.

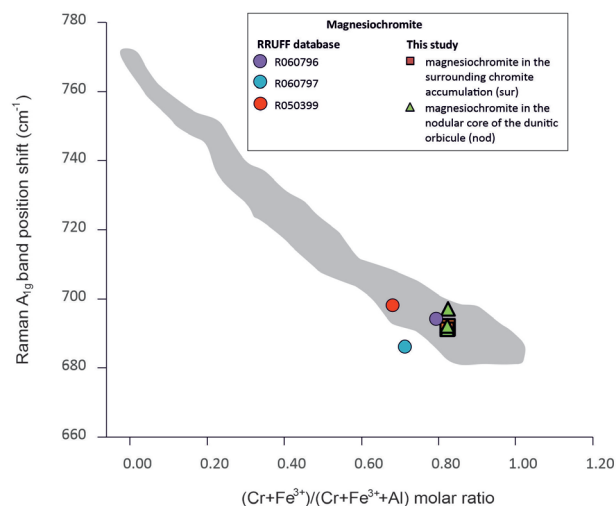


Figure 7. Plot of Raman A_{1g} band position shift vs the $(\text{Cr}+\text{Fe}^{3+})/(\text{Cr}+\text{Fe}^{3+}+\text{Al})$ molar ratio for the studied magnesiochromites. Diagram utilized after Wang et al. (2004) and the gray background data cluster field is established from data points from Wang et al. (2004) and Malézieux and Piriou (1988). A_{1g} band positions and the molar ratio for the RRUFF data points established using data from RRUFF library (<https://rruff.info/magnesiochromite>).

to that of the Type I spectra described (Figure 6 a,f). This emphasizes the importance of the crystallographic orientation in the spectrum morphology, and points to the variable orientations of magnesiochromite crystals in the studied Harmancık sample. The spectrum morphology should correlate with the orientation of the target crystal. Such a variance in crystallographic orientation of the magnesiochromites is expectable in ophiolitic chromitites, as they are almost ubiquitously subjected to textural arrangement and plastic deformation in the mantle concomitantly or after the crystallization. Nevertheless, it is not possible to infer which of the grains studied present the initial crystal orientation as the analysis are made on grains with random orientations. On the other hand, as the majority of the 35 grains analysed show Type I spectra, followed marginally by lower numbers of Type II and finally only a single Type III spectra, one may speculate that the grains showing the Type I spectra correspond to the final orientation induced by the plastic deformation, and Type III and Type II spectra correspond to the initial and transitional stage orientations, respectively.

F_{2g} , E_g and other Un-assigned Modes

Considering the above mentioned band assignment sequence and band positions discussed in the literature,

the low intensity $\sim 605\text{ cm}^{-1}$ shoulder bands in the studied spectra are attributed to the $F_{2g}(3)$ that is similarly regarded as a result of ${}^M\text{BO}_6$ symmetric stretching vibrations (Reddy and Frost, 2005; Marinković Stanojević et al., 2007; Kharbush, 2018). Taking the previous studies in account, the medium intensity band at $\sim 555\text{ cm}^{-1}$ and the broad band at $\sim 470\text{ cm}^{-1}$ are considered to correspond to the $F_{2g}(2)$ bending vibrations (Marinković Stanojević et al., 2007; Kharbush, 2018), and E_g symmetric ${}^M\text{B-O}$ stretching vibrations (Reddy and Frost, 2005; Marinković Stanojević et al., 2007; Kharbush, 2018), respectively. Of these assigned bands, particularly the presence of the $\sim 470\text{ cm}^{-1}$ band and its attribution to the E_g mode is consistent with the inferences of D'Ippolito et al. (2015) and concurrence of Lenaz and Lughì (2017) for this mode to be distinctive for chromate spinels with $\text{Cr}\# > 0.60$.

No bands could be attributed to the $F_{2g}(1)$ mode, which corresponds to the lowest and weakest Raman shift related to the translatory lattice vibrations (Marinković Stanojević et al., 2007; Kharbush, 2018). Moreover, the origins of the $\sim 650\text{ cm}^{-1}$ shoulder, the $\sim 580\text{ cm}^{-1}$ connection, and $\sim 395\text{ cm}^{-1}$ broad bands could not be related with any of the Raman-active vibrational modes of spinel. Such absence of $F_{2g}(1)$ mode, or the presence of unexpected (thus unassigned) bands are also reported in several earlier work elsewhere (e.g. Wang et al., 2002, 2004; Marinković Stanojević et al., 2007; D'Ippolito et al. 2015; Kharbush, 2018). Here, it must also be noted that the Raman shift values of these unassigned peculiar bands in the previous studies (e.g., Kharbush, 2018) are significantly in good agreement with the wavenumber ranges of unassigned bands detected in this study.

To the author's knowledge, there is no detailed discussion on the Raman bands above the 1000 cm^{-1} spectral region for natural spinels in the literature. On the other hand, there are some notes in the synthetic solid-solution studies. McCarty and Boehme (1989), in their Raman spectral characterization study of the systems $\text{Fe}_{3-x}\text{Cr}_x\text{O}_4$ and $\text{Fe}_{2-x}\text{Cr}_x\text{O}_3$, also do not report on any distinctive bands in the higher wavenumbers for the low Cr-bearing members of the spinel solid solutions ($\text{Fe}_{3-x}\text{Cr}_x\text{O}_4$; for $x=0, 0.4, 0.8, 1.2$). However, for the high Cr-bearing members ($x=1.8, \text{ and } 2$), they report a weak broadband at $\sim 1335\text{ cm}^{-1}$, and a peak and a broadband at $\sim 1265\text{ cm}^{-1}$ and $\sim 1357\text{ cm}^{-1}$, respectively, interpreting these high wavenumber bands as overtones or combinations of the fundamental vibrations (McCarty and Boehme, 1989). The high wavenumber bands encountered in the spectra in this current study similarly mimic the behaviour of the overtones reported by McCarty and Boehme (1989). Accordingly, the $\sim 1130, 1285, 1390, \text{ and } \sim 1450\text{ cm}^{-1}$ bands occur approximately 2 times the $555, 650, 690, \text{ and } 730\text{ cm}^{-1}$ wavenumbers,

and thus may be interpreted as overtones of the $F_{2g}(2)$, un-assigned $\sim 650, A_{1g}$, and un-assigned 730 cm^{-1} modes, respectively.

CONCLUSIONS

This first detailed study on characterization of Raman spectra from an ophiolitic chromitite sample from the northern ophiolite belt of Türkiye has revealed descriptive Raman spectral band frequencies for high-Cr chromitites.

1. The studied chromitite sample presents dunitic orbicular texture, semi-massive texture, and massive texture. Magnesiochromite grains show an almost uniform composition reflecting a high-Cr ($\text{Cr}\# > 0.60$) character, and a distinctive boninitic to arc-related affinity.
2. The uniform magnesiochromite chemistry has been considered helpful in constraining the Raman spectral features and interpretation of infrequently observed significant variances in the designated three spectra morphologies (Type I, Type II, and Type III). All of these three spectra types include the same descriptive Raman bands for chromate spinels.
3. Four of the bands (at around $690\text{ cm}^{-1}, 605\text{ cm}^{-1}, 555\text{ cm}^{-1}, \text{ and } 470\text{ cm}^{-1}$) have been assigned to $A_{1g}, F_{2g}(3), F_{2g}(2), \text{ and } E_g$ Raman-active vibrational modes of spinels.
4. An unassigned band at $\sim 730\text{ cm}^{-1}$, described in the literature to be typical for the high-Cr magnesiochromites, has been utilized to detect the differences on crystallographic orientation of the magnesiochromite grains. This observation has been considered as a useful utility for following up the textural arrangement and plastic deformation history of the chromitite.
5. Currently, one of the most used methods for detection of the crystallographic orientations, and/or strain changes, and thus the deformational history of the ophiolitic chromitites is the Electron Backscatter Diffraction (EBSD). However, this study emphasizes that at least a preliminary approach on the crystallographic orientation of the magnesiochromites of the ophiolitic chromitites can also be made via Raman spectroscopy, albeit by constraining the chemical variance variable on the target grains.

ACKNOWLEDGEMENTS

The author is grateful to Aynur Küçük for her efforts on gathering the electron microprobe data, and to Dr. Nusret Kaya for his efforts for the Raman spectroscopic work. Two anonymous reviewers are also thanked for their constructive criticism of the prior version of the paper.

REFERENCES

- Akbaş B., Akdeniz N., Aksay A., Altun İ., Balcı V., Bilginer E., Bilgiç T., Duru M., Ercan T., Gedik İ., Günay Y., Güven İ.H., Hakyemez H.Y., Konak N., Papak İ., Pehlivan Ş., Sevin M., Şenel M., Tarhan N., Türkecan A., Ulu Ü., Uğuz M.F., Yurtsever A. and others, 2001. Geological Map of Turkey. General Directorate of Mineral Reserach and Exploration [Maden Tetkik ve Arama Genel Müdürlüğü - MTA] Publ. Ankara, Turkey.
- Akbulut M., 2018. Investigation of silicate micro-inclusions from Orhaneli and Harmancık chromitites (NW Turkey): New ultrahigh-pressure evidence from western Tethyan ophiolitic chromitites. *Ofioliti* 43, 1-22, doi: 10.4454/ofioliti.v43i1.453.
- Barnes S.J. and Roeder R.L., 2001. The range of spinel compositions in terrestrial mafic and ultramafic rocks. *Journal of Petrology* 42, 2279-2302.
- Bilgrami S.A., 1963. Further data on the chemical composition of Zhob Valley chromites. *The American Mineralogist* 48, 573-587.
- Chopelas A. and Hofmeister A.M., 1991. Vibrational spectroscopy of aluminate spinels at 1 atm and of $MgAl_2O_4$ to over 200 kbar. *Physics and Chemistry of Minerals* 18, 279-293.
- D'Ippolito V., Andreozzi G.B., Bersani D., Lottici P.P., 2015. Raman fingerprint of chromate, aluminate and ferrite spinels. *Journal of Raman Spectroscopy* 46, 1255-1264, doi: 10.1002/jrs.4764.
- Fraas L.M., Moore J.E., Salzberg J.B., 1973. Raman characterization studies of synthetic and natural $MgAl_2O_4$ crystals. *Journal of Chemical Physics* 58, 3585-3592.
- Kaliwoda M., Giordano D., Krüger M.E., Uysal I., Akmaz M.R., Hoffmann V., Hochleitner R., Schmahl W.W., 2021. Raman Spectroscopy as a tool for the quantitative estimation of chromium aluminum oxide content in chromite. *Spectroscopy* 36 (2), 17-23.
- Kamenetsky V.S., Crawford A.J., Meffre S., 2001. Factors controlling chemistry of magmatic spinel: an empirical study of associated olivine, Cr-spinel and melt inclusions from primitive rocks. *Journal of Petrology* 42, 655-671.
- Kharbish S., 2018. Raman spectroscopic features of Al-Fe³⁺-poor magnesiochromite and Fe²⁺-Fe³⁺-rich ferrian chromite solid solutions. *Mineralogy and Petrology* 112, 245-256. doi: 10.1007/s00710-017-0531-1.
- Laetsch T. and Downs R., 2006. Software for identification and refinement of cell parameters from powder diffraction data of minerals using the RRUFF project and American Mineralogist Crystal Structure Databases. 19th General Meet. Intern. Miner. Ass., Kobe, Japan, July 2006. Abstr. 23-28.
- Lenaz D. and Lughi V., 2013. Raman study of $MgCr_2O_4$ - $Fe^{2+}Cr_2O_4$ and $MgCr_2O_4$ - $MgFe_2^{3+}O_4$ synthetic series: the effects of Fe²⁺ and Fe³⁺ on Raman shifts. *Physics and Chemistry of Minerals* 40, 491-498, doi: 10.1007/s00269-013-0586-4.
- Lenaz D. and Lughi V., 2017. Raman spectroscopy and the inversion degree of natural Cr-bearing spinels. *American Mineralogist* 102, 327-332. doi: 10.2138/am-2017-5814.
- Lenaz D. and Skogby H., 2013. Structural changes in the $FeAl_2O_4$ - $FeCr_2O_4$ solid solution series and their consequences on natural Cr-bearing spinels. *Physics and Chemistry of Minerals* 40, 587-595. doi: 10.1007/s00269-013-0595-3.
- McCarty K.F. and Boehme D.R., 1989. A Raman Study of the Systems $Fe_{3-x}Cr_xO_4$ and $Fe_{2-x}Cr_xO_3$. *Journal of Solid State Chemistry* 79, 19-27.
- Malézieux J.M., Barbillat J., Cervelle B., Coutures J.P., Couzi M., Piriou B., 1983. Étude de spineless de synthèse de la série $Mg(CrxAl_{2-x})O_4$ et de chromites naturelles par microsonde Raman-laser. *Tschermaks mineralogische und petrographische* 32, 171-185. doi: 10.1007/BF01081108.
- Malézieux J.M. and Piriou B., 1988. Relation entre la composition chimique et le comportement vibrationnel de spinelles de synthèse et de chromites naturelles en microspectrométrie Raman. *Bull. Minéral.* 111, 649-669.
- Marinković Stanojević Z.V., Romčević N., Stojanović B., 2007. Spectroscopic study of spinel $ZnCr_2O_4$ obtained from mechanically activated ZnO - Cr_2O_3 mixtures. *Journal of the European Ceramic Society* 27, 903-907. doi: 10.1016/j.jeurceramsoc.2006.04.057
- Naveen, Sarkar S., Kumar T.N., Ray D., Bhattacharya S., Shukla A.D., Moitra H., Dagar A., Chauhan P., Sen K., Das S., 2019. Mineralogy and spectroscopy (VIS near infrared and micro-Raman) of chromite from Nidar ophiolite complex, SE Ladakh, India: Implications for future planetary exploration. *Planetary and Space Science* 165, 1-9. doi: 10.1016/j.pss.2018.12.007.
- Nayak B.B., Debata R., Kesavan K., Rath A., Gronen L.H., Sindern S., Wagner T., 2024. Petrography and chemistry of chromite phases from the Mesoarchean chromitite bodies of the Boula-Nuasahi ultramafic complex, India: Indicators of magmatic evolution and hydrothermal alteration. *Mineralogy and Petrology* 118, 231-251. doi: 10.1007/s00710-024-00856-3.
- Reddy B.J. and Frost R.L., 2005. Spectroscopic characterization of chromite from the Moa-Baracoa ophiolitic massif, Cuba. *Spectrochimica Acta A* 61, 1721-1728. doi: 10.1016/j.saa.2004.07.002.
- Rollinson H., 2008. The geochemistry of mantle chromitites from the northern part of the Oman ophiolite: inferred parental melt composition. *Contributions to Mineralogy and Petrology* 156, 273-288.
- Rollinson H. and Adetunji J., 2015. The geochemistry and oxidation state of podiform chromitites from the mantle section of the Oman ophiolite: a review. *Gondwana Research* 27, 543-554. doi: 10.1016/j.gr.2013.07.013.
- Tavlan M., Thorne R., Herrington R.J., 2011. Uplift and lateritization history of the Çaldağ ophiolite in the context of Neo-Tethyan ophiolite obduction and uplift: implications for the Cenozoic weathering history of western Anatolia. *J. Geol.*

- Soc. London 168, 927-940.
- Uysal İ., Akmaz R.M., Kapsiotis A., Demir Y., Saka S., Avcı E., Müller D., 2015. Genesis and geodynamic significance of chromitites from Orhaneli and Harmancık ophiolites (Bursa, NW Turkey) as evidenced by mineralogical and compositional data. *Ore Geology Reviews* 65, 26-41.
- Uysal İ., Şen D.A., Ersoy E.Y., Dilek Y., Saka S., Zaccarini F., Escayola M., Karlı O., 2014. Geochemical make-up of oceanic peridotites from NW Turkey and the multi-stage melting history of the Tethyan upper mantle. *Mineralogy and Petrology* 108, 49-69.
- Yong W., Botis S., Shieh S.R., Shi W., Withers A.C., 2012. Pressure induced phase transition study of magnesiochromite (MgCr_2O_4) by Raman spectroscopy and X-ray diffraction. *Physics of the Earth and Planetary Interiors* 196-197, 75-82. doi: 10.1016/j.pepi.2012.02.011.
- Wang Z., O'Neill H.S.T.C., Lazor P., Saxena S.K., 2002. High pressure Raman spectroscopic study of spinel MgCr_2O_4 . *Journal of Physics and Chemistry of Solids* 63, 2057-2061. doi: 10.1016/S0022-3697(02)00194-4.
- Wang A., Kuebler K.E., Jolliff B.L., Haskin L.A., 2004. Raman spectroscopy of Fe-Ti-Cr-oxides, case study: Martian meteorite EETA79001. *American Mineralogist* 89, 665-680.
- Wang A., Han J., Guo L., Yu J., Zeng P., 1994. Database of standard Raman spectra of minerals and related inorganic crystals. *Applied Spectroscopy* 48, 959-968.
- White W.B. and De Angelis B.A., 1967. Interpretation of the vibrational spectra of spinels. *Spectrochimica Acta* 23A, 985-995.
- Wojdyr M., 2010. Fityk: a general-purpose peak fitting program. *Journal of applied Crystallography* 43, 1126-1128. doi: 10.1107/S0021889810030499.



This work is licensed under a Creative Commons Attribution 4.0 International License CC BY-NC-SA 4.0.